PREDICTION OF PREFERENTIAL CONCENTRATION STATISTICS FROM EULERIAN TWO-POINT CORRELATIONS

Andrew Banko

Department of Mechanical Engineering
Stanford University
Stanford, CA 94305
abanko@stanford.edu

Laura Villafañe

Department of Mechanical Engineering
Stanford University
Stanford, CA 94305
lvillafa@stanford.edu

Mahdi Esmaily-Moghadam

Department of Mechanical Engineering
Stanford University
Stanford, CA 94305

John K. Eaton

Department of Mechanical Engineering
Stanford University
Stanford, CA 94305

ABSTRACT

Non-local statistics of preferential concentration in the inertial range of turbulence are studied by considering the size distribution of high number density regions of particles, "clusters," and low number density regions, "voids". Direct Numerical Simulation is used to compute particle and fluid phase statistics in particle-laden isotropic turbulence and turbulent square duct flow, including the size distributions of clusters and voids. It is found, in agreement with the literature, that clusters are correlated with low enstrophy flow structures and voids with high enstrophy flow structures. Statistical topography is used to predict the size distributions of clusters and voids, which are in good agreement with those computed from the isotropic turbulence simulations. This suggests that the underlying carrier phase turbulence can be used to quantitatively model more complicated statistics of the particle phase in homogeneous and isotropic turbulence. However, the statistical topography methods poorly predict preferential concentration in an anisotropic turbulent square duct flow. The model shortcomings are discussed.

INTRODUCTION

Disperse inertial particles in a turbulent flow become preferentially concentrated, dynamically forming clusters with number densities several times higher than the mean and leaving adjacent regions of the flow completely devoid of particles (Fessler *et al.*, 1994; Balachandar & Eaton, 2010). Studies of preferential concentration are motivated by its persistence across flows with seemingly disparate length and time scales: dust-laden internal cooling passages in jet engines, radiation absorption by rain droplets in clouds, and mass agglomeration in planet forming nebulae. Cluster and void formation arises from the finite aerodynamic time constant, τ_p, of heavy particles which causes their trajectories to deviate from those of the Lagrangian fluid elements. The accepted mechanisms can be concisely summarized by a perturbation expansion assuming small τ_p, an incompressible carrier fluid, and an Eulerian representation of the disperse phase (Maxey, 1987):

$$v_i \approx u_i - St_\eta \left(\frac{Du_i}{Dt}\right) \;;\; \frac{D\ln(n)}{Dt} \approx -St_\eta \nabla^2 p = -St_\eta \left(|\Omega|^2 - |S|^2\right)$$

All above quantities are non-dimensional. Here v_i and n are velocity and number density fields for the particle phase, u_i is the fluid velocity, St_η is the Stokes number based on the Kolmogorov time scale of the turbulence, p is the fluid pressure field, Ω is the rotation rate tensor, and S is the strain rate tensor. The local number density therefore decreases in regions of high rotation rate and low strain, indicating that heavy particles are centrifuged out of the cores of vortices. Conversely, particles accumulate in regions of low vorticity and high strain, and stick to points of zero acceleration (Chen *et al.*, 2006).

There has been significant success in modelling preferential concentration at sub-Kolmogorov scales due to the differentiability of the velocity field across the viscous interval (Balkovsky *et al.*, 2001; Gustavson & Mehlig, 2016). The controlling parameter at viscous length scales is St_η. In general, particles respond to a range of fluid time scales around the aerodynamic time constant, and a scale dependent Stokes number has been used to describe the propensity of particles to preferentially concentrate on length scales larger than the Kolmogorov scale (Yoshimoto & Goto, 2007). Recently, attention has turned to preferential concentration on inertial range scales for its importance in cloud physics and planet formation (Matsuda *et al.*, 2012; Johansen *et al.*, 2007). Much of the current research analyzes and models coarse-grained single point statistics and particle pair statistics, such as the number density probability distribution and the radial distribution function (Bec *et al.*, 2007; Bragg *et al.*, 2015). This is not surprising considering that a complete description specifying the joint probability distribution function (PDF) of position and velocity for N particles is intractable for even small N. However, additional non-local statistics, such as the spatial extent of low particle number density regions (i.e. voids), are important in many systems. For instance, the radar reflectivity factor characterizing the intensity of reflected microwave signals from clouds is determined by the power spectrum of cloud droplet number density fluctuations, a non-local statistic (Matsuda *et al.*, 2014). Several authors calculated the PDF for the sizes of voids in two and three-dimensional turbulence and noted the self-similarity of void sizes in the inertial range, as evidenced by power-law tails of the PDF (Boffetta & Lillo, 2004; Yoshimoto & Goto, 2007). The self-similar distribution of void sizes was attributed to the self-similarity of the turbulence, as voids were found to be correlated with regions of high vorticity magnitude. The power law tail was modeled as $p(V) \sim V^{-16/9}$, where V is the void volume, by assuming a self-similar hierarchy of spherical vortices, devoid of particles, and reproducing a Kolmogorov $-5/3$ energy spectrum.

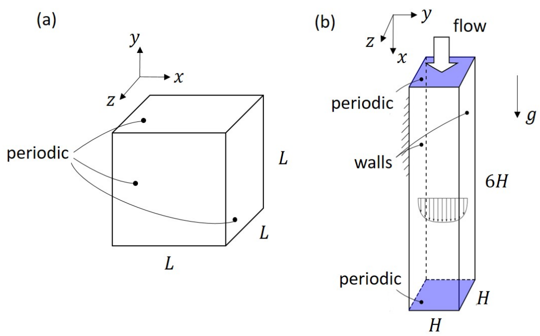

Figure 1. Simulation domains for (a) homogeneous and isotropic turbulence and (b) turbulent square duct flow.

This paper extends the ideas of Yoshimoto & Goto (2007) and quantitatively models the algebraic tails of cluster and void size PDFs using the two-point statistics of scalar fields in the carrier-phase turbulence to which the particle positions are strongly correlated (e.g. enstrophy and the pressure hessian). The theoretical background for the model comes from statistical topography, which describes the properties of isocontours of random scalar functions. The predictions are compared to results from point particle Direct Numerical Simulations (DNS) of homogeneous and isotropic turbulence (HIT). Since HIT is an idealized flow that can never be fully realized in physical systems due to large scale anisotropies such as shear, we also compare the results to the DNS of a turbulent square duct flow. In what follows, we briefly describe the numerical methodology, provide an overview of the important concepts from statistical topography, and then present results from the simulations on cluster and void statistics.

SIMULATION METHODOLOGY

Numerical simulations of particle-laden turbulent flow are performed in order to compute the statistics of particle clusters and voids, examine their correlations with the fluid phase turbulence, and to compare results to the predictions of statistical topography. Two flows are considered: homogeneous isotropic turbulence and turbulent square duct flow.

The Direct Numerical Simulation (DNS) of statistically stationary, homogeneous and isotropic turbulence (HIT) is performed on a triply periodic domain, as shown is Figure 1a. Complete details of the simulation method are given in Esmaily-Moghadam & Mani (2016). The incompressible Navier-Stokes equations are solved on a staggered mesh with 256^3 control volumes. The Taylor Reynolds number is $\mathrm{Re}_\lambda = 100$ and stationarity is maintained using linear forcing with dynamic feedback such that temporal fluctuations in the volume averaged Kolmogorov timescale are less than 0.3%.

The motion of inertial particles is simulated using the point-particle method, wherein discrete particles are tracked in a Lagrangian frame of reference assuming a Stokes drag force. Gravity is neglected and the simulations are one-way coupled meaning that the back-reaction force by the particles on the fluid is ignored. Inter-particle collisions are also neglected. The Kolmogorov based Stokes numbers, which were simulated simultaneously, are $St\eta \equiv \tau_p/\tau_\eta = 2^z$ for $z \in \{-4, -3, ..., 4\}$. For each Stokes number, 10^5 particles were initialized randomly in space and allowed to evolve for several large eddy turnover times before collecting instantaneous snapshots of particle positions and fluid velocity fields for post-processing.

A second one-way coupled, point-particle DNS was done for the pressure driven turbulent flow in a square duct. Figure 1b shows a schematic of the computational domain. The fluid phase is calculated using a staggered scheme on a stretched mesh with 160 control volumes in the wall normal directions and 240 control volumes in the streamwise direction. An aspect ratio of is 6:1 is used in order to ensure that the flow becomes de-correlated in the periodic streamwise direction. The Reynolds number based on the bulk velocity, duct width, and kinematic viscosity is $\mathrm{Re} \equiv U_b H/\nu = 10^4$. A polydisperse collection of particles is simulated in order to match a companion experiment described in ne *et al.* (2017*b*). The Kolmogorov based Stokes numbers computed from the channel averaged dissipation rate are in the range of $St\eta \in (0.5, 8)$, and the average Stokes number is about 5. In this case, the simulations were four-way coupled to include particle-wall and particle-particle collisions, but the mass loading was kept low enough such that two-way coupling between the particles and the fluid is unimportant. Accounting for collisions was necessary in order to counteract the turbophoretic drift of particles towards the walls and establish a statistically stationary concentration distribution. Gravity is included and aligned with the streamwise direction in order to match the experiments; however, the particle settling velocity is two orders of magnitude smaller than the bulk velocity and so the effect of gravity is small. The simulation was allowed to run for several flow through times such that all statistics were stationary prior to collecting snapshots of particle positions and fluid velocity fields for post-processing.

PERCOLATION AND STATISTICAL TOPOGRAPHY OVERIVEW

The goal of the present research is to model the statistics of spatially coherent preferentially concentrated structures. In the same way that turbulent flows are approximately decomposed into vortex sheets and tubes, particle-laden flows have been decomposed into clusters and voids. The clusters correspond to spatially connected regions of high particle number density, and the voids to regions of low particle number density. As with fluid turbulence, there is a freedom of choice in the definition of “high” and “low,” which are typically thresholds on number density specified by the researcher. An additional ambiguity not present in the fluid phase is the definition of number density. The preferentially concentrated, disperse particle phase typically does not satisfy a continuum hypothesis at any scale and therefore the number density depends on the volume over which it is defined (the coarse-graining scale).

Percolation theory provides a framework to approximate the statistics of clusters and voids while simultaneously studying the effect of coarse-graining and threshold. The percolation problem is typically posed on a lattice, in which sites are occupied and unoccupied with a certain probability, and correlations between sites are allowed. Occupied sites connected to occupied nearest neighbors form clusters. Statistical topography is an equivalent framework posed in terms of scalar fields, the closed isocontours of which form the clusters. The values of the scalar field at separate points are correlated because the scalar field is continuous. For percolation theory, the occupation probability represents the threshold and the lattice unit cell represents the coarse graining scale. For statistical topography, the value of the isocontour and the smallest characteristic length scale represent the threshold and coarse graining scale, respectively. As the name suggests, varying the threshold causes clusters to grow and shrink and at some critical level to percolate as shown in Figure 2. In this figure the occupation probability is increased towards the percolation threshold between panels (a) and (c). Correspondingly, the total number of occupied sites shown in black increases. The largest clusters present in panels (a) and (c) are shown in (b) and (d), respectively. Below the percolation threshold, the largest cluster is finite in size (Figure 2b). At the percolation threshold, a cluster on the order of the system dimensions appears (Figure 2d), indicating the presence of long range order. Also at

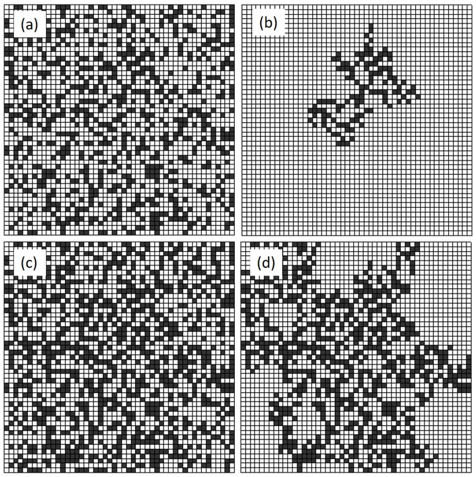

Figure 2. Illustration of the percolation phenomena on a 50 x 50 square lattice. Occupied sites are shown in black and empty sites are shown in white. The total set of occupied sites are plotted in (a) and (c) for two occupation probabilities approaching the percolation threshold: 30% in (a) and 40% in (c). Clusters are defined using 8 nearest-neighbor connectivity. (b) and (d) show the largest clusters present in (a) and (c), respectively. The cluster in (d) is an example of a spanning cluster.

this threshold, it is known that the probability distribution function (PDF) of cluster sizes has an algebraic tail. Above and below the percolation threshold there is still an algebraic tail but with exponential cut-off.

Many of the rigorous results, scaling arguments, and applications of percolation theory and statistical topography are summarized in the review by Isichenko (1992). The conclusions relevant to the present work are succinctly written with respect to multi-scale (i.e. long-range correlated) statistical topography as outlined in Isichenko & Kalda (1991). In multi-scale statistical topography there is a broadband spectrum of length scales present, and in mono-scale statistical topography there is a single length scale present which is on the order of the correlation length.

Consider a scalar field $n(\mathbf{x},t)$ with mean zero as a function of space in two or three dimensions at a fixed time, t. Denote the spectrum of n as $E(k)$ such that $< n^2 >= \int_0^\infty E(k)dk$, assuming statistical isotropy where $k = |\mathbf{k}|$ is the magnitude of the wavevector $\mathbf{k}$. Here $< \cdot >$ denotes the expected value. Then if $E(k) \sim k^{-p}$ we have $2H = p-1$ where H is related to the scaling of the structure function, $S(r)$, or two-point correlation, $R(r)$, of n by the Wiener-Khinchin theorem:

$$S(r) =< (n(r)-n(0))^2 >\sim r^{2H} \quad : \quad 0 < p < 1$$
$$R(r) =< n(r)n(0) >\sim r^{2H} \quad : \quad 1 < p < 3$$

In statistical topography, the clusters form a fractal set. A fractal can have a non-integer dimension because the boundary is rough, and because the set is fragmented into clusters. The number-area rule gives the scaling of the cumulative distribution function for the sizes of clusters based on the fractal dimension. If V is a random variable denoting the d-dimensional volume, then:

$$P(V > \mathrm{v}) \sim \mathrm{v}^{-d_F/d} \text{ or } p(V) \sim V^{-(1+d_F/d)}$$

Where $P(\cdot)$ denotes probability and $p(V)$ is the probability density.

Table 1. Fractal dimension of the set of clusters predicted by statistical topography. The dimension of the space is d. The critical exponents are: $\nu = 4/3$, $\beta = 5/36$ for $d = 2$; $\nu \approx 0.85$, $\beta \approx 0.42$ for $d = 3$

$H < -1/\nu$	$-1/\nu < H < 0$	$0 < H < 1$
$d - \beta/\nu$	$d + \beta H$	$d - H$

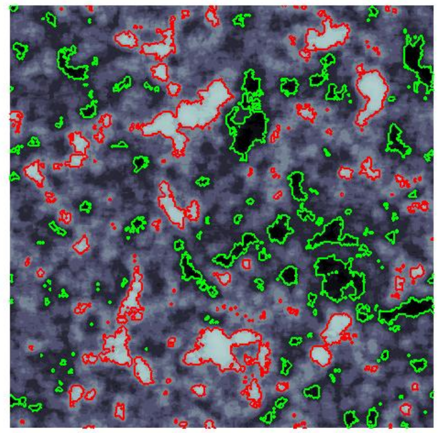

Figure 3. Snapshot of particle number density field calculated with a filter width of $R/\eta = 7$. Clusters (red) and voids (green) are outlined for thresholds applied near the percolation threshold.

Therefore, by knowing the scaling of the two-point correlations, or equivalently the power spectrum, one can predict the distribution of cluster sizes.

Statistically topography predicts that the fractal dimension, d_F, of the set of clusters is equal to the fractal dimension of free isocontours given in Table 1. H is related to the strength of the correlations. If $-1/\nu < H < 1$ then correlations are long range enough to be important, and if $H < -1/\nu$ then the problem reduces to that of mono-scale statistical topography (which is equivalent to the uncorrelated lattice percolation problem).

SIMULATION COMPARISON AND DISCUSSION

This section presents cluster/void results from the simulations with direct comparison to the model predictions. Number density fields are computed from the simulations at several times, t. The coarse grained number density assigned to each computational grid cell is defined as the number of particles within a ball of radius R centered on that cell, divided by the volume of the ball. If there are N particles in the simulation and the i^{th} particle is located at $\mathbf{x}_{\mathbf{p}_i}$: $n(\mathbf{x},t) = \frac{1}{\mathrm{Vol}(B_R)} \int_{B_R(\mathbf{x})} \left(\sum_{i=1}^N \delta(\zeta - \mathbf{x}_{\mathbf{p}_i})\right) d^3\zeta$.

Clusters are then defined as connected components of the set of points for which $n_R(\mathbf{x},t)$ is greater than or equal to $\alpha \in \mathbb{R}_{\geq 0}$ standard deviations from the mean. Likewise, voids are defined as the connected components of the set of points for which $n_R(\mathbf{x},t)$ is less than or equal to $\beta \in \mathbb{R}_{\geq 0}$ standard deviations from the mean. Figure 3 shows an example of clusters and voids identified from the HIT simulation near the percolation threshold. The figure is a cross-sectional slice through the three-dimensional structures.

In order to predict the sizes of particle clusters and voids, we assume that particle positions are strongly correlated with a scalar field in the flow whose two-point correlation (or spectrum) is known from the DNS. We then use the statistical topography results to identify an appropriate fractal dimension and power law tail of the size PDF.

Isotropic Turbulence

A range of particle Stokes numbers were considered in the simulations. It was found that the results are insensitive for all $St_\eta > 2$, because each of these Stokes numbers exhibit preferential concentration on scales greater than the Kolmogorov scale and up to the integral scale of the turbulence. Therefore for brevity and to improve statistics we combine the Stokes numbers 2, 4, and 8 into a single set of particles for each snapshot. Particle clusters and voids are then computed across several snapshots. Finally, any clusters and voids intersecting a boundary of the simulation domain are reconnected using the periodicity of the simulation to structures on the opposite boundary.

First, we briefly describe the effect of the threshold and coarse-graining scale on the number and size of clusters/voids identified in the simulation. Qualitatively, the observations will be similar to the picture of percolation described previously in Figure 2. When the threshold is close to the mean number density, a spanning cluster and void exist for all coarse-graining scales. As the threshold is increased, eventually all structures become finite in size. We remark that the critical threshold at which this transition happens is relatively independent of the scale over which number densities are computed and close to 1.5 standard deviations from the mean, for both the clusters and the voids. The maximum size of the finite clusters and voids peaks when the spanning structure becomes finite, and the volume then shrinks as the thresholds are further increased. Also, the number of objects decrease with increasing threshold and increasing coarse-graining scale due to the elimination of small clusters and voids. The number of objects also decreases slightly for thresholds very near the mean number density because smaller clusters and voids combine into larger ones.

The results for clusters/voids larger than the coarse-graining scale were found to be insensitive to most choices of R. If R was too close to the system dimensions, then the results were biased. Likewise, if R was too small (i.e. comparable to the mean particle spacing) then a large number of small structures reminiscent of Poisson noise appeared. Therefore for brevity, the following results correspond to $R/\eta = 7$, which is an intermediate value. We also limit the discussion to thresholds near the critical threshold when the spanning cluster disappears.

As discussed in the introduction, previous studies have shown that individual particles tend to be concentrated in regions of the flow with low vorticity and high strain rate, or equivalently $\nabla^2 p < 0$. Figure 4 shows scatter plots of the average enstrophy and the average pressure hessian computed over each cluster and void. The results are in good agreement with this conclusion, especially for the largest clusters and voids. Smaller structures may be the result of Poisson noise due to the finite number of particles, and these structures are not as well separated into dynamically distinct regions of the flow.

The PDF of cluster and void sizes are shown in Figure 5a. In agreement with Yoshimoto & Goto (2007), voids can be orders of magnitude larger than the Kolmogorov scale of the turbulence. This is also true for the clusters, which have a very similar size PDF. In order to predict the algebraic tail of the PDFs, power spectra of the coarse-grained number density, enstrophy, and pressure hessian are calculated from the simulations. Due to the relatively low Taylor Reynolds number, it was found that all spectra decay exponentially. Therefore, the problem simply reduces to that of mono-scale statistical topography. The implied fractal dimension is $d_F \approx 2.51$

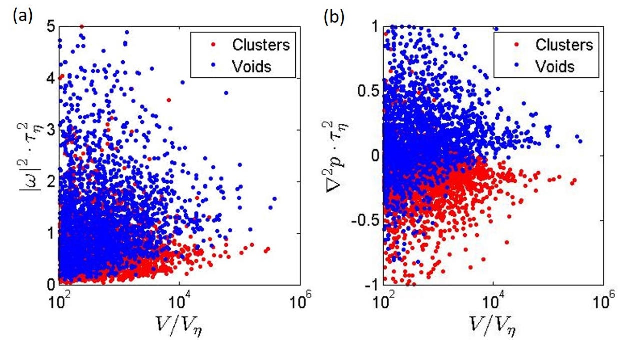

Figure 4. (a) Scatter plot of average enstrophy, $|\omega|^2$, and (b) average pressure hessian, $\nabla^2 p$, computed over each cluster and void in HIT. The coarse graining scale $R/\eta = 7$. The enstrophy and pressure hessian are normalized by the Kolmogorov time scale, τ_η, and the cluster/void volumes are normalized by the volume of the Kolmogorov scale, $V_\eta = \eta^3$.

and the PDF of both clusters and voids are expected to scale as $p(V) \sim V^{-1.84}$. This prediction is plotted as the solid line in Figure 5a, and is a good approximation to the tail of both PDFs. For comparison, Yoshimoto & Goto (2007) used an alternative argument to predict $p(V) \sim V^{16/9} \approx V^{-1.77}$, which corresponds to a smaller fractal dimension of $d_F = 2.33$. Due to the present statistical uncertainty, it is difficult to rule out either power law exponents and additional data should be collected so that parameter estimation can be performed.

Figure 5b and 5c show the size PDFs of regions of high and low enstrophy, and positive and negative pressure hessian for comparison. The high enstrophy and positive pressure hessian curves are similar to that of the particle voids, and are also modeled well by the statistical topography prediction. This is in agreement with the previous observation that voids are on average in regions of high vorticity and low strain rate. The PDFs of low enstrophy and negative pressure hessian decay slightly faster than that of the clusters and the model, but range of sizes and decay of the tail are still comparable.

The results from HIT suggest that the size distributions of clusters/voids, and low/high regions of enstrophy, and negative/positive regions of pressure hessian are similar. The fact that mono-scale statistical topography provides a reasonable prediction for the cluster/void size PDFs is interesting because it is based on a fractal description of the fields. For Stokes numbers greater than 2, Esmaily-Moghadam & Mani (2016) found that the particles at sub-Kolmogorov length scales are not concentrated onto a fractal set. The present results therefore provide additional evidence that preferential concentration above and below the Kolmogorov scale can be fundamentally different. We also note that the fractal description also suggests that the particle structures possess some degree of self-similarity despite the fact that the turbulence does not contain a self-similar inertial range.

Turbulent Square Duct Flow

The same analysis is repeated for the turbulent square duct flow in order to examine the effect of large scale anisotropy. In an experiment using the same distribution of particles, duct dimensions, and Reynolds number, ne *et al.* (2017*a*) found that particle clusters possessed a preferred orientation towards the principal mean shear direction. The post-processing methods applied to the DNS data are the same as for the HIT simulations except that only the central 3/4 of the duct is used. This excludes the regions close to the walls were

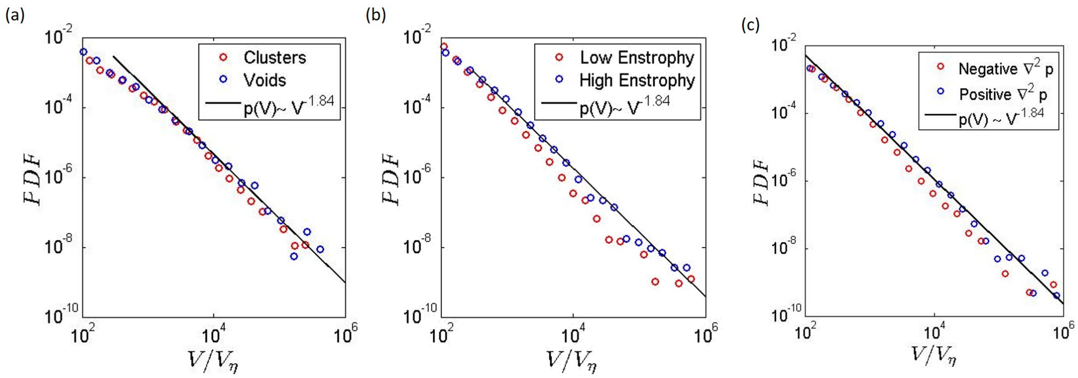

Figure 5. (a) Probability distribution of cluster and void volumes, and (b) probability distribution of the volumes of high and low enstrophy regions, (c) probability distribution of the volumes of positive and negative pressure hessian regions in HIT. The volumes are normalized by the volume of the Kolmogorov scale, $V_\eta = \eta^3$. The solid line is the prediction from mono-scale statistical topography.

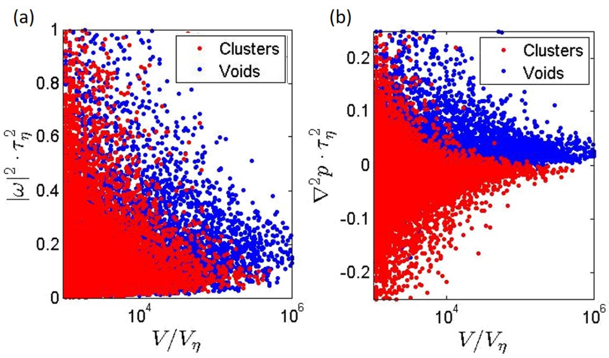

Figure 6. (a) Scatter plot of average enstrophy, $|\omega|^2$, and (b) average pressure hessian, $\nabla^2 p$, computed over each cluster and void in the duct flow. The coarse graining scale $R/\eta = 7$. The enstrophy and pressure hessian are normalized by the Kolmogorov time scale, τ_η, and the cluster/void volumes are normalized by the volume of the Kolmogorov scale, $V_\eta = \eta^3$.

turbophoresis increases the mean concentration distribution. Clusters and voids intersecting the boundaries of this sub-domain are excluded from the statistics. The percolation properties were qualitatively similar to those from the HIT simulation, and for brevity we present results at a similar coarse-graining scale of $R/\eta = 8.3$ and near the percolation threshold.

Figure 6 is a scatter plot of enstrophy and pressure hessian averaged over each cluster and void. The pressure hessian shows a similar separation between clusters and voids to that of HIT: large clusters tend to have $\nabla p < 0$ and voids have $\nabla p > 0$. However, there is more overlap between the set of cluster and void points than in HIT. This is most clearly observed in the scatter plot of the enstrophy. The largest voids occur in regions with distinctly higher enstrophy, but for each cluster size there is also a corresponding void with a similar level of enstrophy.

The differences between the HIT and duct cases become more apparent when considering the size distributions of clusters and voids as shown in Figure 7. While the structures span a similar range of scales compared to the Kolmogorov scale of the turbulence, the decay of the PDF is distinctly different for clusters and voids. The cluster PDF approximately follows a power-law with an exponent similar to that predicted by the mono-scale statistical topography. The mono-scale result is used because the 1-dimensional power spectra computed in the streamwise direction for number density, enstrophy, and pressure heassian decay exponentially due to the low Reynolds number of the flow (not shown here).

The void PDF, on the other hand, decays more slowly than the model prediction for $V/V_\eta \sim O(10^4)$. For larger void sizes, the linear extent of the structures become comparable to the domain cross-sectional dimensions and the rate of decay of the PDF increases. Therefore, the scaling of size distributions of clusters and voids in the duct flow are different from one another, whereas they were indistinguishable in HIT. This observation is approximately reflected in the size PDFs of regions of high and low enstrophy for $V/V_\eta \sim O(10^4)$. However, the influence of the finite domain cross-section becomes apparent at values of $V/V_\eta > 10^4$. It is possible that large structures extend from the near wall region as observed for Reynolds stress structures in the study of Lozano-Duran *et al.* (2012), and therefore are likely to be excluded from the statistics because they intersect the domain boundaries. The size PDFs of pressure hessian for positive and negative values have similarly shaped tails, which decay more slowly than the model for $V/V_\eta < 10^4$ and then very rapidly for $V/V_\eta > 10^4$. This can be due to the intersection of large structures with the domain boundaries as well. The slow decay of the void size PDF is qualitatively reflected in pressure hessian PDFs, but the resemblance is not as striking as that obtained in HIT. The pressure Hessian PDFs also do not distinguish between the sign of the pressure hessian, while the particle cluster and voids showed different behavior from one another.

Overall, the simple statistical topography model fails to predict the scaling of cluster and void sizes in the turbulent duct flow. This is not surprising given the fact that the isotropy assumption is broken, and it warrants the need for further study of preferential concentration in anisotropic and inhomogeneous flows.

CONCLUSIONS

We have presented results from the DNS of particle-laden isotropic turbulence and turbulent square duct flow. The statistics of particle clusters and voids were calculated as a means for investigating the non-local properties of preferential concentration. It was found, in agreement with previous studies, that clusters are concentrated in regions of the flow with low vorticity and high strain rate. Conversely, voids were correlated with regions of high vorticity and low strain. Although this is true in both flows, the clusters and voids showed a less obvious decomposition in the duct.

The distribution of cluster and void sizes were calculated from the simulations and compared to predictions from statistical topography. Due to exponential decay of the power spectra for the particle number density, fluid enstrophy, and fluid pressure hessian fields, the percolation problem fell into the class of mono-scale statistical

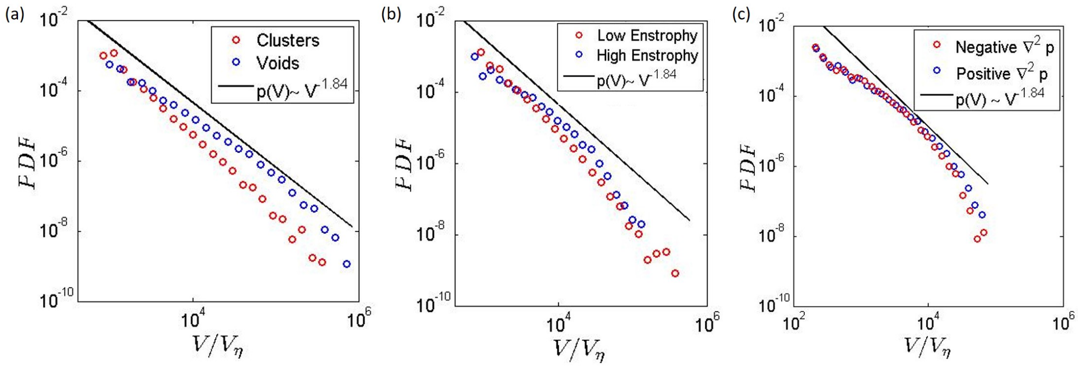

Figure 7. (a) Probability distribution of cluster and void volumes, and (b) probability distribution of the volumes of high and low enstrophy regions, (c) probability distribution of the volumes of positive and negative pressure hessian regions in the duct flow. The volumes are normalized by the volume of the Kolmogorov scale, $V_\eta = \eta^3$. The solid line is the prediction from mono-scale statistical topography.

topography. In HIT, the size PDFs of all quantities displayed heavy algebraic tails that were well approximated by the mono-scale statistical topography prediction. This suggests a sort of symmetry in the statistics of clusters and voids, in addition to a strong correspondence with the background turbulence structures.

The symmetry between cluster and void size statistics was broken in the turbulent duct flow case, and statistical topography provided a poor approximation of the void size PDFs. This is because the model assumes statistical isotropy of the scalar field under analysis, and does not explicitly depend on the isocontour of interest (e.g. positive or negative). Therefore it could not capture the difference between clusters (positive number density fluctuations) and voids (negative number density fluctuations).

Future work should investigate the mechanism responsible for differences in the statistics of clusters and voids in anisotropic flows in order to better predict preferential concentration in engineering systems. Simulations of HIT should also be performed at higher Reynolds numbers in order to achieve an inertial range and test the predictions of multi-scale statistical topography. With a sufficient Reynolds number it may also be possible to distinguish between inertial range scales at which a variety of Stokes numbers cluster similarly, and scales at which the clustering is different.

REFERENCES

Balachandar, S. & Eaton, J.K. 2010 Turbulent dispersed multiphase flow. *Annu. Rev. Fluid Mech.* **42**, 111–133.

Balkovsky, E., Falkovich, G. & Fouxon, A. 2001 Intermittent distribution of inertial particles in turbulent flows. *Phys. Rev. Letters* **86**, 2790–2793.

Bec, J., Biferale, L., Cencini, M., Lanotte, A., Musacchio, S. & Toschi, F. 2007 Heavy particle concentration in turbulence at dissipative and inertial scales. *Phys. Rev. Letters* **98**, 084502.

Boffetta, G. & Lillo, F. De 2004 Large scale inhomogeneity of inertial particles in turbulent flows. *Phys. of Fluids* **16**, 20–23.

Bragg, A.D., Ireland, P.J. & Collins, L.R. 2015 Mechanisms for the clustering of inertial particles in the inertial range of isotropic turbulence. *Phys. Rev. E* **92**, 023029.

Chen, L., Goto, S. & Vasssilicos, J.C. 2006 Turbulent clustering of stagnation points and inertial particles. *J. Fluid Mech.* **553**, 143–154.

Esmaily-Moghadam, M. & Mani, A. 2016 Analysis of the clustering of inertial particles in turbulent flows. *Physical Review Fluids* **1**, 084202.

Fessler, J.R., Kulick, J.D. & Eaton, J.K. 1994 Preferential concentration of heavy particles in a turbulent channel flow. *Physics of Fluids* **6**, 3742–3749.

Gustavson, K. & Mehlig, B. 2016 Statistical models for spatial patterns of heavy particles in turbulence. *Advances in Physics* **65**, 1–57.

Isichenko, M.B. 1992 Percolation, statistical topography, and transport in random media. *Reviews of Modern Physics* **4**, 961–1043.

Isichenko, M.B. & Kalda, J. 1991 Statistical topography. i. fractal dimension of coastlines and number-area rule for islands. *Journal of Nonlinear Science* **3**, 255–277.

Johansen, A., Oishi, J.S., Low, M.M., Klahr, H., Henning, T. & Youdin, A. 2007 Rapid planetesimal formation in turbulent circumstellar disks. *Nature Letters* **448**, 1022–1025.

Lozano-Duran, A., Flores, O. & Jimenez, J. 2012 The three-dimensional structure of momentum transfer in turbulent channels. *J. Fluid Mech.* **694**, 100–130.

Matsuda, K., Onishi, R., Hirahara, M., Kurose, R., Takahashi, K. & Komori, S. 2014 Influence of microscale turbulent droplet clustering on radar cloud observations. *Journal of the Atmospheric Sciences* **71**, 3569–3581.

Matsuda, K., Onishi, R., Kurose, R. & Komori, S. 2012 Turbulence effect on cloud radiation. *Phys. Rev. Letters* **108**, 224502.

Maxey, M.R. 1987 The gravitational settling of aerosol particles in homogeneous turbulence and randow flow fields. *J. Fluid Mech.* **174**, 441–465.

ne, L. Villafa Banko, A.J., Kim, J.H., Elkins, C.J. & Eaton, J.K. 2017*a* Effect of mass loading and stokes number on preferential concentration of inertial particles in a turbulent square duct flow. *In preparation* .

ne, L. Villafa Banko, A.J., Kim, J.H., Elkins, C.J. & Eaton, J.K. 2017*b* Effect of radiative heating of inertial particles in a particle-laden turbulent square duct flow. In *Proceedings of 10th International Symposium on Turbulence and Shear Flow Phenomena*. Chicago, IL.

Yoshimoto, H. & Goto, S. 2007 Self-similar clustering of inertial particles in homogeneous turbulence. *J. Fluid Mech.* **577**, 275–286.